Conference Proceedings

EuroSun 2016
Palma de Mallorca (Spain), 11 - 14 October 2016

Experimental Investigation of Water Evaporation for Closed Adsorption Storage Systems

Bao Nam Dang[1], Wim van Helden[1], Michael Olbricht[2] and Andrea Luke[2]

[1] AEE - Institute for Sustainable Technologies, Gleisdorf (Austria)

[2] University of Kassel, Kassel (Germany)

Abstract

Closed adsorption for thermal energy storage is a promising technology, which was recently proven on real scale. Nevertheless further improvements of its material and components are necessary to enhance the system performance and to make it economically viable. One of the issues is the evaporation of water at low pressure during discharging ("adsorption") of the storage. The current lack of accurate experimental data and correlations for the heat transfer coefficient makes the design of the evaporator difficult. Therefore the goal of the work is to gather deeper knowledge in order to design the evaporator more properly and thus improve the sorption storage efficiency. In this work a test rig was designed and constructed for the experimental investigations of water evaporation at sub-atmospheric pressure. For the commissioning, first experiments with falling film evaporation were conducted on a copper tube bundle (3 x 8 tubes) to determine the relation of the outer heat transfer coefficient to different parameters. In all experiments the observed flow patterns between the tubes consist of columns. Varying the saturation pressure from 20 to 23 mbar or the range of the $Re_{\dot{I}}$ 29 to 109 shows no effects. Apart from that, the measured results were compared to values from two correlations. It is concluded that the Nu numbers from the measurements were in good agreement with those from the Lorenz and Yung model.

Keywords: closed adsorption thermal storage, falling film evaporation, water

1. Introduction

Efficient seasonal thermal energy storages are necessary to cover all the domestic heat demand with solar thermal energy over the whole year. An innovative and proven concept in real scale - the solid sorption heat storage - uses the reversible adsorption/desorption process of water vapor in zeolite 13XBF. This material pair provides a significantly higher energy density S (theoretically: 250 kWh/m³) compared to water. In general a sorption storage system consists of one or more vessels with the sorption material, a condenser/evaporator and a water reservoir. For loading the storage ("desorption") the moist zeolite is dried by the heat from solar collector and the emerging vapor is condensed and stored separately in a water tank (Fig. 1a).

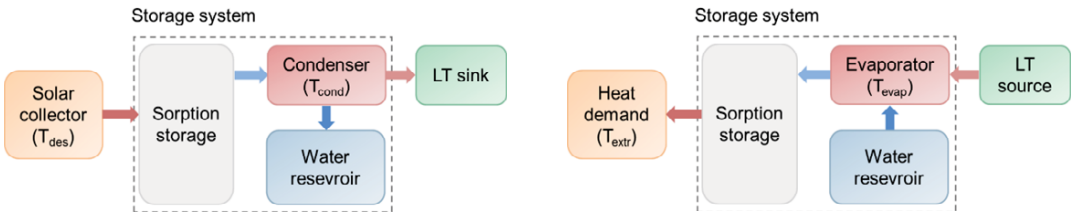

Fig. 1: Scheme of the sorption storage system during desorption (a) and adsorption (b)

doi:10.18086/eurosun.2016.03.09 Available at http://proceedings.ises.org

Regardless of the sensible heat, the thermal sorption energy can be stored over months virtually without losses. To discharge the sorption storage, the distilled water is evaporated at low temperature using the heat of the low temperature source. The vapor will be adsorbed by the zeolite and the resulting heat from the adsorption can be used for domestic hot water, space heating or other purposes (Fig. 1b). In reality the storage is limited by the operation conditions and cannot be fully charged or discharged. Because the storage system is evacuated, the pressure difference drives the vapor transport between the sorption storage and the heat exchanger for evaporation/condensation, and depends on the temperature in the single components. In order to achieve a high material energy density, a maximal desorption (T_{des}) and a minimal condensation temperature (T_{cond}) is required during the desorption as well as a maximal evaporation (T_{evap}) and a minimal extraction temperature (T_{extr}) during the adsorption process. This means an efficient evaporator with high heat transfer leads to smaller temperature overheating and thus a higher evaporation temperature, which as a result enhances the energy density and the storage efficiency (Tab. 1). This coherence was also verified by our closed adsorption storage system for a single-family house from the "COMTES"-project, which was operated successfully during the last heating period from October 2015 to January 2016. Further improvement of the evaporator is only possible with a thorough knowledge of the evaporation process of water at low pressures. (Engel, 2016) (Köll, 2016)

Tab. 1: Material energy density (*S*) of zeolite 13XBF. (In all cases: T_{des} = 180 °C and T_{extr} = 25 °C) (Köll, 2016)

T_{evap}	*S* (T_{cond} = 17°C)	*S* (T_{cond} = 25 °C)	*S* (T_{cond} = 35 °C)
10 °C	126 kWh/m³	115 kWh/m³	106 kWh/m³
15 °C	146 kWh/m³	135 kWh/m³	126 kWh/m³
20 °C	150 kWh/m³	139 kWh/m³	130 kWh/m³

In recent years the experimental studies on water evaporation with different concepts and at temperatures from 5 to 20 °C has been intensified. Still, there is a lack of accurate experimental data. Furthermore there are many known and unknown factors, which influence each other and have a different impact depending on the prevailing conditions. These are the heat flux density, the fluid properties, the saturation pressure, the roughness and the material of the heating surface, the dimension of the apparatus and operation-specific parameters. In sum, the proper design and the improvement of the evaporation of water at low temperatures is currently imprecise and troublesome. One of the main issues for water as refrigerant is the local saturation pressure with p_{evap} = 8.7 to 23.4 mbar, which also depends on the liquid level above the heating surface. Due to the hydrostatic pressure of the water, the pressure increases around 0.98 mbar per cm ($\Delta p = \rho \cdot g \cdot \Delta h$). For example, a flooded evaporator operates at 10 °C with a corresponding pressure of 12.3 mbar. Its heating surface lays 3 cm deep under the water level, which causes a hydrostatic pressure of 2.9 mbar. Hence the local saturation pressure is 15.2 mbar and the temperature 13 °C. This temperature increase can immensely diminish the evaporation power. Because of this concepts with evaporating thin liquid films are preferred to minimize the hydrostatic pressure effect, like the falling film and the capillary assisted evaporation.

Recently the capillary assisted evaporation is increasingly investigated. Its working principle is using capillary structured or coated heating surfaces, which are partly immersed into the refrigerant pool. Due to the capillary forces a thin liquid film covers the surface passively, so no further active components like pumps are necessary. However, the heat transfer coefficient still depends heavily on the liquid level. In addition the long-term functionality is not clear, because fouling can easily accumulate in the capillaries and limit the capillary forces. Overall these evaporators are less complex and have lower weight. But they are probably more suitable for systems with low volume of the refrigerant capacity. (Bahrami, 2016) (Xia, 2007) Falling film-type evaporators with horizontal tubes have been used in different applications like desalination, refrigeration and air conditioning. Furthermore their functionality is also proven for absorption cooling systems. In contrast to the large falling film evaporators like in the food or pharmaceutical industry, the evaporating liquid film will be sprayed or dropped on to the top of a horizontal tube bundle. So the film falls gravitational from tube to tube redistributing itself on each tube again. Therefore a good alignment of the tubes and the proper liquid distribution are required in order to maintain the wetting of the heating surfaces area and thus an efficient evaporation. Especially for deep bundles it is difficult to have a consistent flow and prevent local dry outs. Although it is more complex, this type of evaporator works with much less refrigerant and has higher performances than flooded evaporators. Due to the thin liquid layer with inner turbulences,

the evaporation occurs by natural convection with low surface overheating. Therefore the falling film evaporation seems to be suitable for the application of the seasonal sorption storage and will be experimentally investigated in this work. (Ribatski and Jacobi, 2005) (Thome, 2009)

2. Experimental design and procedure

The goal of this work is to experimentally determine the heat performance $\dot{Q}_{evap}$ and the heat transfer coefficient h_o of a falling film evaporator at certain conditions. Therefore a test rig was designed and built that is similar to the apparatus of Li (2010a, 2010b) or Olbricht (2013, 2016). As shown in Fig. 2, it consists of a cylindrical evacuated vessel, containing the test tube bundle. The vessel contains also temperature sensors and a pressure sensor for measuring the conditions inside. On top of the bundle is the feeding system, which is fed from a water reservoir (in Fig. 2: Reservoir 1). This reservoir collects all the surplus water that is not evaporated at the bundle. To minimize the liquid pool at the bottom of the vessel, tilted plates below the tube bundle channel the water to the drain. Meanwhile the vapor from the evaporator will be drawn off into a plate heat exchanger, where it condenses and falls into a second reservoir. Both reservoirs are hydraulically connected to each other, so shifting the amount of water between the both reservoirs is possible. As seen in the Fig. 2, each of them consists of two differently sized tanks, where the smaller contains a liquid level sensor. Depending on the valve control between the two tanks, the liquid level in the smaller tank and in the vertical tube, which parallel to the tank, is measured with or without the level in the bigger tank. Overall there are three liquid circuits in the test rig: the water used for the evaporation (refrigerant), the water circuit for heating the tube bundle from the inside and the cooling water circuit for the condensation. The last two of these are connected via heat exchangers to our laboratory's hot water and cold water circuit. They are also equipped with sensors for measuring the inner flow's inlet and outlet temperature and the volumetric flow rate.

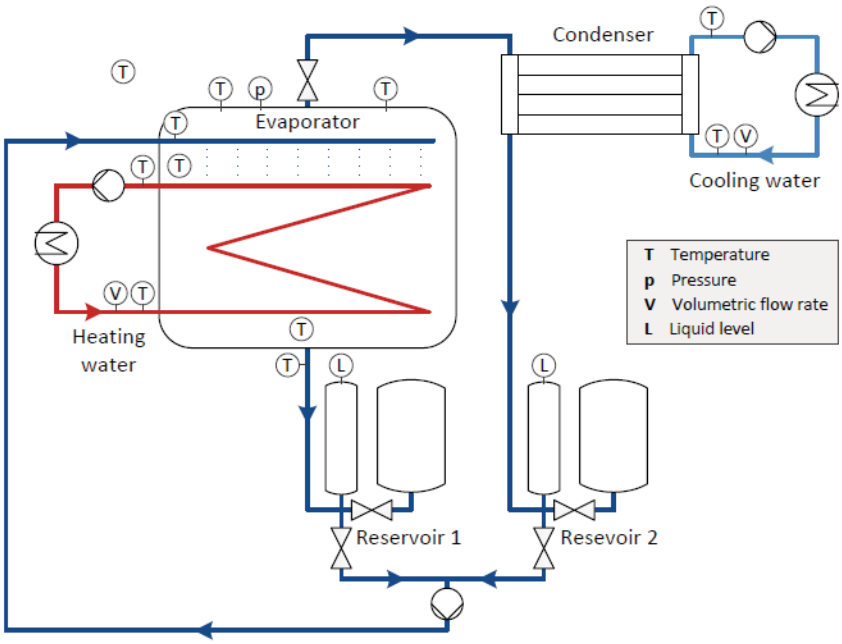

Fig. 2: Scheme of the test rig

The tested tube bundle is similar to the bundle of Olbricht (2013, 2016). It consists of three parallel tube rows, whose outer and inner diameters are 12.70 mm and 12.04 mm (Fig. 3). Both sides of the tube surfaces are plain and not processed. Each single tube row is eight columns high with a center to center tube spacing of 31.75 mm and the inlet and outlet are all connected to the bigger header tube. The liquid feeder is shown in Fig. 4. It consists of three parallel tubes, perforated at the bottom, where the sub cooled refrigerant drops out into a closed box. The box's floor consists of 3 x 39 small pipes, which are all vertically positioned and arranged directly over each tube row of the bundle. The pipe diameter is 1 mm and the spacing is 10 mm. In

addition, all the pipes jut out around 3 mm at both floor's side, so water drains out gravitationally of the box, when there is a small liquid pool in it.

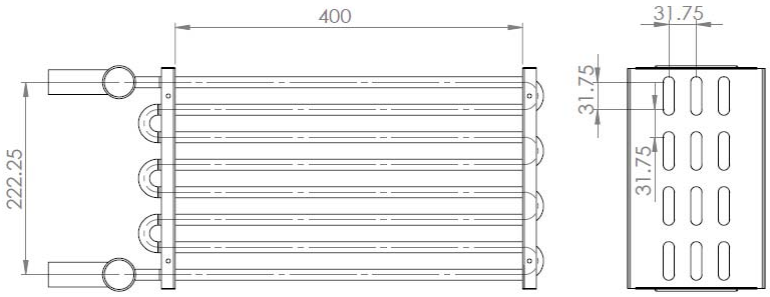

Fig. 3: Sketch of the tube bundle

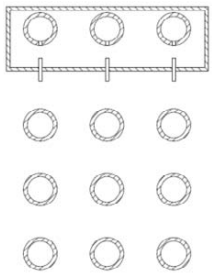

Fig. 4:Sectional view of the liquid feeder

Before the experiment starts, the refrigerant will be conditioned below the saturation pressure, such that when it leaves the feeder it will not evaporate directly until it gets heated by the tube bundle. This will be checked with one temperature sensor inside the feeding tubes and two sensors at the drain of the vessel. During the experiments the inlet temperature of the heating ($T_{hw,in}$) and cooling water ($T_{cw,in}$) are maintained constant. The volumetric flow rate for the refrigerant and the heating water is also set. For controlling the pressure inside the vessel, a PD controller changes the flow rate of the cooling water in the condenser. Tab. 2 shows the setting temperatures, which were set at the examined saturation pressures.

Tab. 2: Setting temperature for each pressure condition

p_{evap}	$T_{\mathrm{H_2O,liq}}$	$T_{hw,in}$	$T_{cw,in}$
20 mbar	17 °C	23 °C	9 °C
23 mbar	19 °C	25 °C	9 °C

Furthermore in each pressure condition, the irrigation density for the refrigerant has been also varied over a range of 0.007 to 0029 kg/(ms), which correspond to a $Re_{\dot{\Gamma}}$ from 29 to 107.

3. Measurement evaluation

There are two different options to measure the performance of the evaporator at stationary conditions. The first option is by measuring the temperatures and the volumetric flow rate of the heating and cooling water. With these values the heat flow at each component can be calculated.

$$\dot{Q}_{hw} = \dot{m}_{hw} \cdot c_{p_{hw}} \cdot \left(T_{hw,in} - T_{hw,out}\right) \quad \text{(eq. 1)}$$

$$\dot{Q}_{cw} = \dot{m}_{cw} \cdot c_{p_{cw}} \cdot \left(T_{cw,in} - T_{cw,out}\right) \quad \text{(eq. 2)}$$

Another method is using the liquid level of the reservoirs. During the measurements, all the valves at Reservoir 2 are closed. So the liquid levels in the vertical tube from the condenser and in the smaller tank rise. The heat flow can then be determined with the change of the liquid volume per time, the liquid density and the vapor enthalpy of water.

$$\dot{Q}_{rv2} = \Delta \mathrm{H}_{\mathrm{H_2O},vap} \cdot \rho_{\mathrm{H_2O,liq}} \cdot \dot{\mathrm{V}}_{\mathrm{H_2O,liq}} \quad \text{(eq. 3)}$$

Ideally, the three measured heat flows should be equal. But because the ambient of the test rig cannot be conditioned, heat gains or losses need to be considered when calculating the evaporation performance. For this, the thermal heat transfer coefficient of the vessel and the condenser was identified. Overall the experiments show that the results of all three measurement methods for the evaporation performance $\dot{Q}_{evap}$. With the temperature difference between the mean temperature of heating water flow and the saturation

temperature of the refrigerant, the overall heat transfer coefficient UA can be calculated. Taking it into account, the results of all three measurement methods for the evaporation power $\dot{Q}_{evap}$were in good agreement.

$$UA = \frac{\dot{Q}}{\Delta T} \qquad \text{(eq. 4)}$$

In all measurement the Reynolds number of heating water inside the tubes was in the range of 5600 to 5900. So for calculating the convection heat transfer coefficient h_i, the relations of Gnielinski (2010) for the transition region between laminar and turbulent flow are used:

$$Nu_i = (1-\gamma)\cdot Nu_{lam,2300} + \gamma \cdot Nu_{tur,10^4} \qquad with \qquad \gamma = \frac{Re - 2300}{7700} \qquad \text{(eq. 5)}$$

The mean outer heat transfer coefficient h_o, which is the heat transfer coefficient of the falling film evaporation, can be calculated by using the tube's thermal resistance formula.

$$h_o = \frac{1}{d_o \cdot \left(\frac{\pi \cdot l_{tube}}{UA} - \frac{1}{h_i \cdot d_i} - \frac{1}{2 \cdot k_{tube}} \cdot \ln\left(\frac{d_o}{d_i}\right)\right)} \qquad \text{(eq. 6)}$$

For the complete measurement evaluation, the irrigation density $\dot{\Gamma}$and the associated Reynolds number $Re_{\dot{\Gamma}}$ are also calculated with the following equations. In this case $\dot{m}_{H_2O,liq}$ is the total mass flow which is used for wetting the total tube length of the bundle l_{tube}.

$$\dot{\Gamma} = \frac{\dot{m}_{H_2O,liq}}{2 \cdot l_{tube}} \qquad \text{(eq. 7)}$$

$$Re_{\dot{\Gamma}} = \frac{4 \cdot \dot{\Gamma}}{\mu_l} \qquad \text{(eq. 8)}$$

4. Experimental results

At constant saturation pressure condition and with a fixed flow rate for the heating water inside the tubes, the irrigation density or the Reynolds number for the falling film was gradually reduced. As seen in Fig. 5a, the flow pattern between the tubes with low irrigation density consists of droplets and very thin columns. These columns remain only for a few seconds, then they shortly break up and subsequently form again mostly at the same place. With increasing irrigation density more columns occur, which are also thicker (Fig. 5b). However, they exist only for a few seconds, too. Apart from that, few liquid droplets or jets do not fall vertically on the next below tubes. Because of the high flow velocity at the radial edge of the tubes, they will be deflected and fall diagonally. This happens at every experimental setting and mainly at the first three top tube rows, when the liquid falls with too high momentum. Furthermore, very few local dried out spots can be identified at every condition. Mostly they are at the lowest tube rows or at the longitudinal ends of the tubes. A change of number and size of the dried out spots was not visible with different parameter settings.

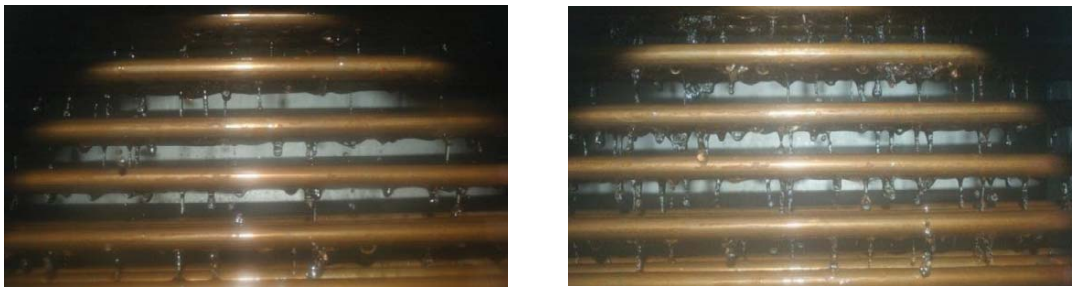

Fig. 5: Flow pattern during measurements with low (a) and high irrigation (b)

Fig. 6 depicts the measured outer heat coefficient in dependency of the saturation pressure and the Reynolds Film number. In our investigated range for $Re_{\dot{\Gamma}}$, the outer heat coefficient at the tubes maintains nearly constant. Similar measurement results can be also found from Li (2010a, 2010b). Furthermore reducing the saturation pressure does not have any effect on the heat coefficient in our experiments, because all deviations are within the accuracy of the measurements. This can be expected as a small difference in pressure, which is equivalent to small temperature changes, leads to very small alteration of the water's properties.

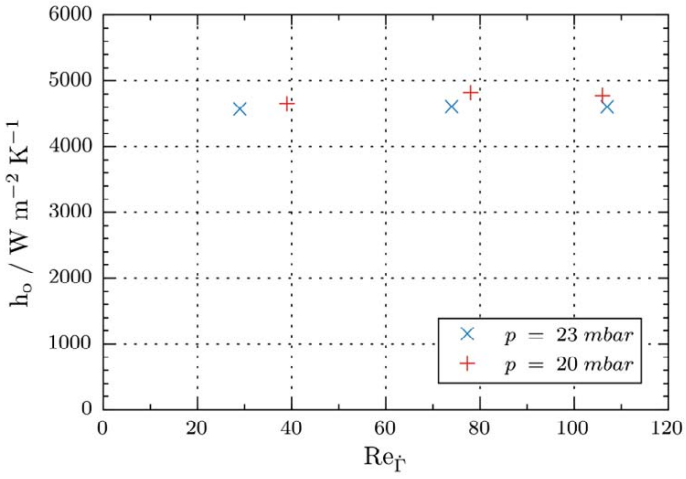

Fig. 6: Results of the measurements at 23 mbar and 20 mbar.

For comparing the measurement results, two correlations were used. The first one is from Hu and Jacobi (1996), where the different types of flow patterns are considered and can be identify by $Re_{\dot{\Gamma}}$. In our case with a Re_{Γ} between 29 and 107, the droplet flow model can be used. The Nusselt Number for this flow pattern can be calculated with the following formulas. Here, D is the outer diameter of the tubes and S is the center to center spacing between two of them.

$$Ar = \frac{D^3 \cdot g}{\nu^2} \qquad \text{(eq. 9)}$$

$$Nu_{\dot{\Gamma},droplet} = 0{,}113 \cdot Re_{\dot{\Gamma}}{}^{0{,}85} \cdot Pr^{0{,}85} \cdot Ar^{-0{,}27} \cdot \left(\frac{S-D}{D}\right)^{0{,}04} \qquad \text{(eq. 10)}$$

The other empirical model is from Lorenz and Yung and is described by Thome (2009). Instead of using several empirical equations for each flow pattern, the heat transfer coefficient is described by a combined model for the evaporation of a subcooled $h_{\dot{\Gamma},dev}$ and of a saturated film $h_{\dot{\Gamma}}$ and the nucleate boiling h_{nb}:

$$h_o = h_{\dot{\Gamma},dev} \cdot \frac{L_{dev}}{L} + h_{\dot{\Gamma}} \cdot \left(1 - \frac{L_{dev}}{L}\right) + h_{nb} \qquad \text{(eq. 11)}$$

where L is the circumference of a single horizontal plain tube and L_{dev} is the developing length of the film, which is calculated by the Nusselt theory for liquid films. The ratio of both lengths is calculated by this equation:

$$\frac{L_{dev}}{L} = \frac{\frac{\dot{\Gamma}^{\frac{4}{3}}}{4 \cdot \pi \cdot \rho \cdot a} \cdot \sqrt{\frac{3 \cdot \mu}{g \cdot \rho^2}}}{\pi \cdot D} \quad . \qquad \text{(eq. 12)}$$

The falling saturated film is calculated by the model of Chun and Seban, which consists of two empirical equations for determining the laminar and the turbulent heat transfer in the evaporating film. For predicting the type of the film flow the Weber Number (We) can be used. In all measurements We was lesser than 1, so the liquid film is laminar and will be calculated with the following equation:

$$h_{\dot{\Gamma},lam} = 0{,}821 \cdot \left(\frac{\mu_l^2}{g \cdot \rho_l^2 \cdot k_l^3}\right)^{-0{,}33} \cdot Re_{\dot{\Gamma}}{}^{-0{,}22} \quad . \qquad \text{(eq. 13)}$$

The heat transfer coefficient of the film's developing region $h_{\dot{\Gamma},dev}$ can be determined with this equation.

$$h_{\dot{\Gamma},dev} = 0{,}375 \cdot c_p \cdot \frac{\dot{\Gamma}}{L_{dev}}. \qquad \text{(eq. 14)}$$

In our experiments, nucleate boiling did not appear and its heat transfer coefficient h_{nb} can be ignored. Therefore only the heat coefficients of the film evaporation are used for calculating with (eq. 12). With the resulting overall heat transfer coefficient of the evaporation film, the associated Nu will be determined.

$$Nu = \frac{h_O}{k} \cdot \left(\frac{\nu^2}{g}\right)^{\left(\frac{1}{3}\right)} \quad . \qquad \text{(eq. 15)}$$

As shown in the diagram of Fig. 6a, there are huge discrepancies between the measurements results and the correlation of Hu and Jacobi, especially at low irrigation density. However at $Re_{\Gamma} > 100$ the values match well. Another point to note is the deviation with the flow pattern. As already mention we observed a column flow patterns between the tubes, which did not change with varying the irrigation density. But according to this model and with a $Re_{\dot{\Gamma}}$ ranging from 29 to 107 it should be droplet flow. A possible reason for this is the different liquid feeder, which was used in Hu and Jacobi's experiments. They used a feeder tube, which has a row of small holes along the bottom, and placed a second tube directly underneath it to help distribute the flow. It has to be assumed that with this configuration the water falls with lower momentum on to the tubes than with the feeding system in this work. However, the empirical results from Lorenz and Yung's correlation are in good agreement with our measurements (see Fig. 6b). Still further detailed investigations are needed to justify the results.

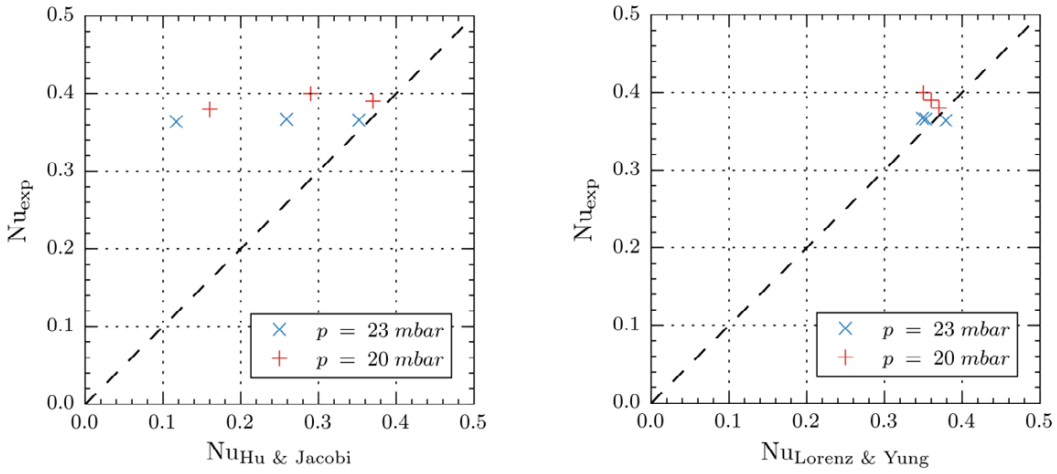

Fig. 7: Comparing measurements results with the correlation of Hu and Jacobi (a) and of Lorenz and Yung (b)

Apart from that, it has to be point out that the determination of the outer heat coefficient depends heavily of the identification of the heating water's inner heat coefficient h_i and of the corresponding temperature difference for calculating the overall heat transfer coefficients UA. Because every other experimental work use different correlations or assumptions, so it can be troublesome to compare with other results and correlations. So for future precise measurements, it will be of interest to heat the irrigated tubes electrically and to measure simultaneous their temperatures.

5. Conclusion

A test rig for experimental investigation of the falling film evaporation was designed and built. For the commissioning, first measurements on a plain copper tube bundle were conducted and evaluated at saturation pressure of 20 and 23 mbar. Varying the falling film Reynolds number in a range from 29 to 109 changes the flow pattern from droplets-columns to columns. However, the heat transfer coefficient for the film evaporation remains nearly constant. This was also observed, when the saturation pressure was differed with unchanged other settings. The experimental data were also compared with values from two empirical models. The comparison shows discrepancies with the correlation of Hu and Jacobi, especially at smaller irrigation density. However, the measurement results were in good agreement with the correlation of Lorenz and Yung. Still, further precise measurements are necessary to justify the results.

In future, further experiments need to be carried out with larger parameter density and range, like the irrigation density. Moreover, experiments at lower saturation pressure can be conducted. Another point is to test with a similar feeder system like from Hu and Jacobi, to check the reason of the discrepancy in this work. Finally, a critical point is the heating water flow, which has large influence on the determination of the evaporation film heat coefficient. Theoretically the flow mode is in the transition region, but it could be also more turbulent due to the elbows in the bundle. So for precise measurement results, experiments with electrical heating tubes and temperature sensors at the tubes should be considered. To sum up, this and all upcoming works are necessary for designing and operating efficient evaporators, which then will be beneficial for sorption storage systems and also other sorption applications, like cooling and heat pumps.

6. Acknowledgements

This research was funded by the project “Solar Heat Integration Network” (SHINE), which is part of the Marie Curie program of the European Union. We thank all our colleagues from AEE - Institute for Sustainable Technologies and the Institute of Technical Thermodynamics at the University of Kassel. Furthermore we want to thank the company Luvata UK Ltd. for manufacturing the tube bundle.

7. Reference

Bahrami, M., 2016. Effects of capillary-assisted tubes with different fin geometries on the performance of a low-operating pressure evaporator for adsorption cooling system applications. Journal Applied Energy, Volume 171, 2016, pp. 256–265.

Engel. G. et al., 2016. Demonstration of a Real-scale Hardware-in-the-loop Seasonal Solar Sorption Storage System. Proceeding: 10th International Renewable Energy Storage Conference, Düsseldorf.

Gnielinski, V., 2010. Heat transfer in pipe flow, in: VDI heat atlas. Book., Düsseldorf, pp. 693-699.

Hu, X. and Jacobi, A.M., 1996. The intertube falling film: Part 2 – Mode effects on sensible heat transfer to a falling liquid film. Journal of Heat Transfer, Vol. 118, pp. 626-633.

Köll, R. et al., 2016. Demonstration of a seasonal sorption storage system in real scale. Proceeding: Otti Conference of Thermal energy storage, Neumarkt, pp. 37-39.

Li, W. et al., 2010a. Falling film evaporation of water on horizontal configured tube bundles. Proceeding: International Heat Transfer Conference, Washington DC.

Li, W. et al., 2010b Falling water film evaporation on newly-designed enhanced tube bundles. International Journal of Heat and Mass Transfer 54 (2011), pp. 2990-2997

Olbricht, M. et al., 2013. Design and commissioning of an absorption chiller. Proceeding: German Society of Refrigeration and Air Conditioning Conference, Hannover.

Olbricht, M. et al. 2016 Heat and Mass Transfer in a Falling Film Evaporator with Aqueous Lithium Bromide Solution. Proceeding: 7th European Thermal-Sciences Conference, Krakau.

Ribatski, G. and Jacobi, A.M., 2005. Falling-film evaporation on horizontal tubes - a critical review. International Journal of Refrigeration, Vol. 28(5), pp. 635-653.

Thome J.R., 2009. Falling film evaporation, in Engineering data book III. Book., pp. 14/1-14/39.

Xia Z.Z. et al. 2007. Experimental investigation of capillary-assisted evaporation on the outside surface of horizontal tubes. International Journal of Heat Mass Transfer 51 (2008), pp. 4047-4054.